Predicting Brain Age in Functional Neuroimages using Node Centrality Measures

Monireh Taimouri University of Cincinnati USA taimoumh@mail.uc.edu Vikram Ravindra University of Cincinnati USA vikram.ravindra@uc.edu

Abstract

Aging is known to be accompanied by structural changes in the brain. This is observed in both healthy subjects and those with neurodegenerative diseases. These anatomical alterations influence functional dynamics. More specifically, changes in structural networks lead to shifts in functional network organization. In this study, we use functional imaging data from individuals aged 18-88 to reveal substantive and sustained gradual changes in functional networks across the human lifespan. Our analysis demonstrates that PageRank - a node centrality measure, effectively captures age-related changes in the brain's functional network. As PageRank is the stationary distribution of random walks, changes due to aging can thus be directly linked to changes in centrality properties (i.e., the importance) associated with different brain regions. We use these PageRank vectors in a trajectory analysis framework to accurately predict the brain ages of subjects. We also present results from other centrality measures and other relevant methods to demonstrate the significance of our results. This work lays the foundation for identifying novel biomarkers crucial to characterizing healthy aging and neurodegenerative diseases.

CCS Concepts

• Computing methodologies → Network science; Image representations; • Applied computing → Life and medical sciences.

Keywords

functional connectomics, network science, aging

ACM Reference Format:

Monireh Taimouri and Vikram Ravindra. 2025. Predicting Brain Age in Functional Neuroimages using Node Centrality Measures. In *Proceedings of the 16th ACM International Conference on Bioinformatics, Computational Biology, and Health Informatics (BCB '25), October 11–15, 2025, Philadelphia, PA, USA.* ACM, New York, NY, USA, 9 pages. https://doi.org/10.1145/3765612. 3767213

1 Introduction

Neuroimages have been an integral source of data for studying human brains. The structures of different areas of the brain and

Permission to make digital or hard copies of all or part of this work for personal or classroom use is granted without fee provided that copies are not made or distributed for profit or commercial advantage and that copies bear this notice and the full citation on the first page. Copyrights for components of this work owned by others than the author(s) must be honored. Abstracting with credit is permitted. To copy otherwise, or republish, to post on servers or to redistribute to lists, requires prior specific permission and/or a fee. Request permissions from permissions@acm.org.

 $BCB~'25, Philadelphia, PA, \, USA$

© 2025 Copyright held by the owner/author(s). Publication rights licensed to ACM. ACM ISBN 979-8-4007-2200-4/2025/10 https://doi.org/10.1145/3765612.3767213

their associated functional properties have been long studied to understand underlying biological processes, as well as to characterize the changes to these processes associated with development, healthy aging, injury and different diseases. Structural neuroimages are high-resolution 3D images showing brain regions and highlighting differences such as white and gray matter. Examples of structural modalities include structural Magnetic Resonance Imaging (MRI) and diffusion MRI (dMRI). Functional neuroimages are 4-dimensional, with three spatial dimensions and one temporal dimension. Examples include functional MRI (fMRI) and Magnetic Encephalography (MEG).

While the spatial resolution of functional images is typically poorer than structural images, the time dimension allows these images to capture the dynamic activity of the brain, thereby elucidating underlying functional processes active at rest, or while performing cognitive tasks. Functional images are often studied in the form of networks called "functional connectomes". In this network, nodes represent brain regions, and edges link regions with similar temporal activity at rest, or in response to external stimuli. As these responses are measured across time, we can view edges as linking pairs of regions with high similarity in neuronal activity. The exact measure of brain activity depends on the imaging technique – for instance, in Blood Oxygen Level Dependent functional Magnetic Resonance Imaging (BOLD fMRI), brain activity is measured as a hemodynamic response by each region to its corresponding neuronal activity.

Over the lifespan, the human brain undergoes structural changes associated with age. These anatomical alterations are expected to influence functional organization, leading to observable differences in functional connectomes. A model capable of capturing age-related patterns would have to be able to predict the brain age from a suitable representation derived from the corresponding neuroimage [5][10][33]. Based on this central idea, we demonstrate that network centrality measures of functional networks drawn from fMRIs serve as useful graph representations that encode age-specific network properties. Specifically, we show that Pagerank vectors extracted from functional networks of healthy subjects aged 18 to 88 effectively capture age-related trends. Next, by treating each subject's PageRank vector as a node in a population-level graph, we propose a method to order subjects according to their ages. This framework achieves competitive performance in predicting brain age across the lifespan. Additionally, we compare the results obtained using different centrality measures, including a) PageRank, b) degree, c) eigenvector, and d) betweenness measures. Finally, we compare our methodology with other approaches from relevant literature to demonstrate that network properties of brains strongly encode age-related information.

The rest of the paper is organized as follows: In Section 2.1, we describe the publicly available large-scale dataset used for this study. Section 2.2 provides details regarding fMRI preprocessing – steps vital to ensuring that noisy brain images are cleaned and amenable to downstream analyses. Sections 2.3 and 2.4 introduce the required concepts of PageRank and trajectory analysis. Sections 3.1-3.4 describe the three core results in this paper. Finally, we conclude our paper with the related literature and discussion in Sections 4 and 5, respectively.

2 Materials and Methods

We begin this section with a description of the Cam-CAN dataset, followed by details of the necessary preprocessing steps required to facilitate downstream analysis. Next, we provide relevant details of the methodological frameworks required for our approach. Specifically, we discuss PageRank centrality, which represents each functional connectome and pseudotime ordering, which allows us to predict the subject's brain age.

2.1 Dataset Description

In this paper, we use the dataset collected by the Cambridge Centre for Ageing and Neuroscience (Cam-CAN) consortium [22][27]. Specifically, we show results from the Cam-CAN Stage 2 study cohort 1 . This dataset is a substantially large publicly available resource for investigating age-related changes in cognition and brain function. Cam-CAN Stage 2 includes multimodal image data, including structural and functional modalities as well as high temporal resolution modalities like Magnetic Encephalography (MEG). It also provides non-imaging data, such as cognitive-behavioral and demographical data, collected from a cohort of $\sim\!650$ individuals spanning the adult lifespan (from 18 to 88 years). By sampling a diverse population, this dataset enables a comprehensive characterization of healthy cognitive aging, focusing on understanding age-related alterations in brain structure, function, and cognitive performance.

2.2 Preprocessing Steps

The functional MRI data utilized in this study underwent artifact and noise removal by the dataset curators. More detailed information regarding the dataset and preprocessing is available in the studies conducted by Shafto et al. [22] and Taylor et al. [27]. In this study, we use the Craddock Atlas [4], which defines 840 functional regions included in the dataset. Our choice for using the Craddock Atlas is guided by the fact that network measures are better estimated on larger graphs, which in our context translates to finer parcellation (i.e., where individual brain regions occupy lesser volume). In addition to the standard preprocessing pipeline, we computed wavelet transforms of all parcellated time-series. Specifically, we use the Best-localized Daubechies filter ('bl10' in MATLAB). We observed that these post-processed time-series enhanced the detectability of age-related features.

2.3 Pagerank Centrality

Pagerank Centrality was first developed to quantify the relative importance of different webpages in a network of webpages (like WWW)[17][2]. Given a graph \mathcal{G} with n nodes and corresponding adjacency matrix \mathbf{A} , the page-rank centrality of the i-th node, denoted as y_i can be expressed as:

$$y_i = \alpha \sum_{j=1}^n \mathbf{A}_{ij} \frac{y_j}{k_j^o} + \beta \tag{1}$$

Here, $A_{ij}=1$ if there is an edge from node j to node i, k_j^o represents the out-degree of the j-th node. If a node has no outgoing edges, k_j^o is set to 1 to avoid divide-by-zero errors. α is a free parameter that must be smaller than 1, and β ensures all nodes (including those with no out-degrees) have non-zero probabilities.

In matrix terms, we can rewrite the previous equation to

$$y = \alpha \mathbf{A} \mathbf{D}^{-1} y + \beta \mathbb{1} \tag{2}$$

Rearranging, we get

$$y = (\mathbf{I} - \alpha \mathbf{A} \mathbf{D}^{-1})^{-1} \mathbb{1},\tag{3}$$

where D is the out-degree matrix defined as

$$\mathbf{D}_{ij} = \begin{cases} \max(\sum_{k} \mathbf{A}_{ki}, 1) & i = j \\ k & \text{otherwise} \end{cases}$$

This definition ensures that all diagonals are non-zero. Additionally, we set $\beta=1$.

Pagerank is a variant of the Eigenvector Centrality, except for the scaling by k_j^o . It is similar to Katz Centrality in the sense that we give a small amount of centrality β for free to each node to ensure that all nodes have non-zero centralities [16]. Pagerank Centrality can be interpreted as the stationary distribution of random walks on the corresponding graph [17]. Thus, $y_i \geq 0 \ \forall i \in \{1,\ldots,n\}$ and $\sum_{i=1}^{n} y_i = 1$.

Pageranks of Brain Networks: As the output of the preprocessing steps mentioned in Section 2.2, we obtain a *(regions x time)* time-series matrix for each subject and each task. For each such matrix, we compute the Pearson Correlation (PC) between all pairs of regions to obtain a *(regions x regions)* matrix, often referred to as the "Functional Connectome (FC)". We sparsify this matrix by retaining the top z% values in the FC to obtain functional networks. We compute the pagerank vectors of these networks. In our experiments, we set $z=\{5,10\}$ as these are common values in practice [7, 12, 20, 21]. results reported in Section 3 are for z=10, as the downstream results are consistent for both values of z.

In the context of our problem setting, we aim to understand changes to the functional activity of the brain in response to structural changes caused by aging. We hypothesize and show that these changes in functional activity are encoded in network properties such as random walks on functional networks. In other words, changes to brain structure can be tied to changes to centrality measures, or *relative importance* of different regions. Thus, they have the potential to serve as reliable biomarkers to characterize aging.

¹https://cam-can.mrc-cbu.cam.ac.uk/dataset/

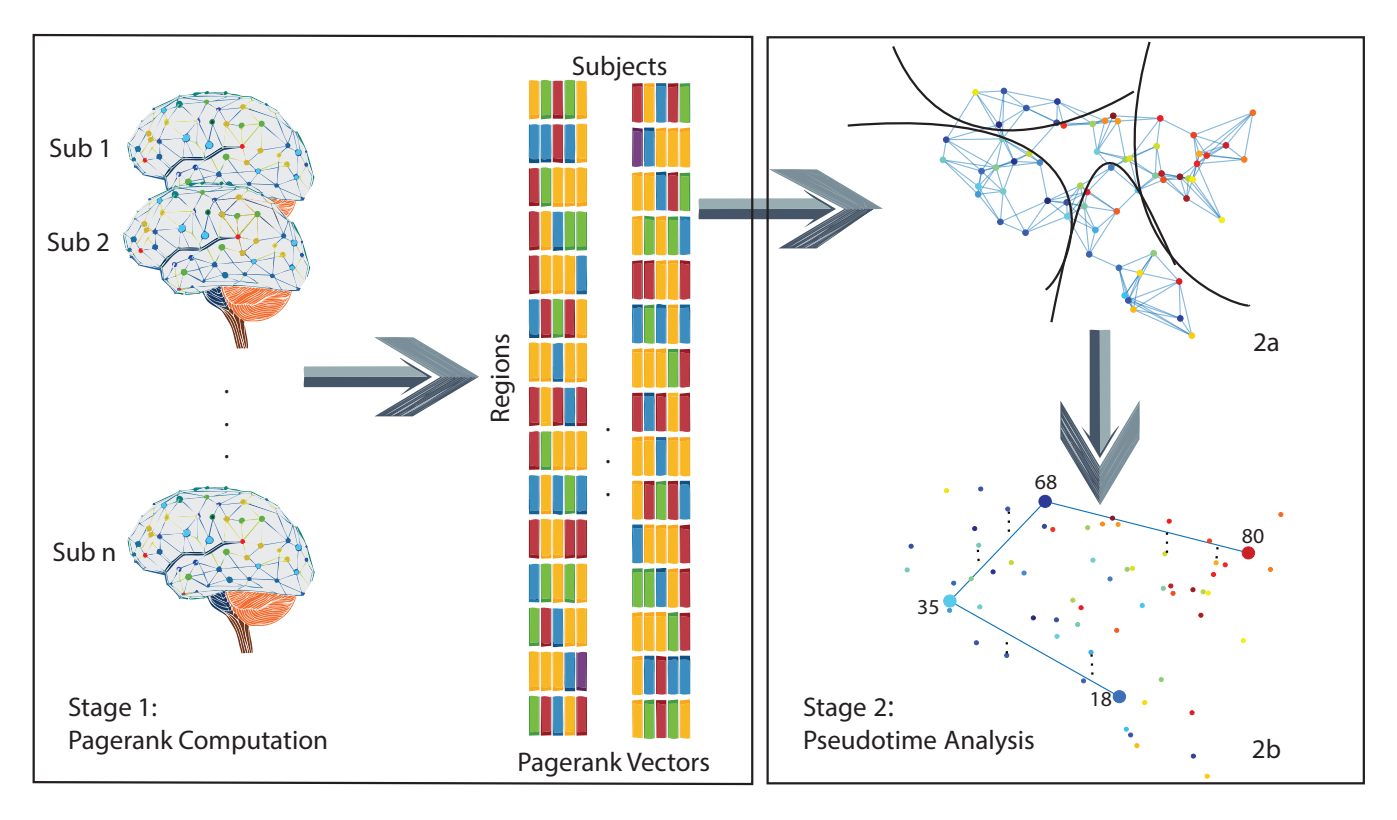


Figure 1: Schematic Representation of our approach. In Stage 1, we compute pagerank vectors from functional networks as explained in Section 2.3. For each subject, this results in a (regions x 1) vector. We stack these vectors into a matrix. In Stage 2a, we compute a population network using k-NN and use spectral clustering to partition nodes (subjects). The partitions are shown with the black curves. Finally, in Stage 2b, we find the "backbone" (shown with blue lines), and project all subjects onto the backbone. Using only the ages of the subjects along the backbone, we can predict ages of all other subjects. Details for Stage 2 are provided in Section 2.4. In this visualization, we have subsampled the data for clarity. The full results are presented in detail in Section 3.

2.4 Pseudotime Analysis

Given an unordered dataset, Pseudotime Analysis refers to techniques that find ordering of data-points. This ordering is used to define a pseudotime "age" or "score". Pseudotime algorithms have been developed to infer progression of cells through biological process such as development or differentiation. Graph-based methods [9, 28] typically proceed by creating a graph/tree from the given dataset, where the nodes represent stages of progression and the edges represent transition between the different stages. In our setting, we know the chronological (actual) ages of the subjects. Our goal is to characterize the progression of brain age as encoded in their functional brain networks. We develop our variant of pseudotime trajectory analysis inspired by [9], wherein the pseudotime score/age is the predicted brain age. If the pagerank vectors for functional networks computed in the previous step accurately captures network changes due to healthy aging, it is reasonable to expect that this predicted brain age should correspond closely to the chronological age. We now describe our pseudotime procedure:

Step 1: Clustering We begin by using k-NN on the pagerank vectors to represent the entire dataset as a graph. Each node in this population graph is a subject, and an edge represents pairs

of subjects whose pagerank vectors are sufficiently similar. We compute the Laplacian Matrix of the graph and perform k-means on the rows of the eigenvector matrix. This effectively performs *spectral clustering*, dividing the dataset into k-clusters. For each cluster i, we denote the subject closest to the center as C_i .

Step 2: Backbone Creation Next, we use the ages of subjects corresponding to the k cluster centers (i.e., C_i) to order the clusters. This is the only place where we utilize the age of cluster-centers as labels. In all, we will use $k \ll n$ ages and predict the ages of the remaining individuals in the same clusters. Denoting the ordered cluster centers as $\{C_1, \ldots, C_k\}$, we compute the edges (i.e., lines) between successive cluster centers as

$$E_{ij} = \frac{C_j - C_i}{||C_j - C_i||_2} \tag{4}$$

where j = i + 1. The path $E_{1,2} - E_{2,3} - E_{3,4} - \cdots - E_{k-1,k}$ is the "backbone" on which we project all other data points. As j = i + 1 always, each cluster C_i has 2 edges associated with it, namely $E_{i-1,i}$ and $E_{i,i+1}$.

Step 3: Projection onto Backbone Then, we project each data point onto the backbone as follows. Data points belonging to clusters 1 and k are projected onto $E_{1,2}$ and $E_{k-1,k}$ respectively. For all intermediate clusters i (1 < i < k), if subject s with pagerank vector M_s belongs to cluster C_i , we compute projections w.r.t both edges associated with C_i . Thus, we compute $p_{i,i+1}^s$ and $p_{i-1,i}^s$, where

$$p_{i,j}^s = |E_{i,j}^T M_s| \tag{5}$$

We identify the edge corresponding to $\max(p_{i,i+1}^s, p_{i-1,i}^s)$. As dot products measure similarity, this edge is uniquely identified. We consider only magnitude because we don't differentiate between $E_{i,i+1}$ and $-E_{i,i+1}$ (= $E_{i+1,i}$). For data-points projected onto the same edge, the order is determined by the magnitudes of the projection on the edge.

Step 4: Predict Age We append the ordering of subject across edges, which gives us the global ordering for the dataset. As each edge has known ages associated with its endpoints, we predict the ages of the subjects along an edge by performing a linear interpolation between the end points. Here, we simply use the fact that each point on a line is a convex combination of its end-points. Comparing the true age with the predicted age gives us an estimate of the error.

The strength of this framework is allowing for a weakly supervised approach to accurately ascertain the age of a subject without having to explicitly train with age as labels. While studying atypical aging, the local neighborhood in the ordering for a subject may be indicative of abnormalities in brain function when compared to neighbors. Finally, as the ordering represents a gradual transition in age, as characterized by changes to stationary probabilities in different brain regions, we can construct branches to represent changes to the functional network brought about by neurodegenerative diseases that accompany aging for many people. However, as our focus is on healthy aging, we do not explore these ideas within the scope of this paper.

2.5 Summary of Our Approach

Starting from preprocessed time-series data obtained from the procedure detailed in Section 2.2, we compute PCs for each subject and for each task. Then, we sparsify the PCs to obtain FCs. We perform PageRank on each FC to compute a distinct *regionsx*1 vector for each suject and each task as described in Section 2.3.

For each task, we perform spectral clustering on the pagerank vectors of all subjects to find clusters of subjects whose PageRank vectors are similar. We designate the subject closest to the center of each of these clusters. Using the age of the cluster centers, we order the clusters (and thereby the corresponding subjects). To find the order of subjects within a cluster, we find the "backbone" and project all subjects onto the backbone as explained in Section 2.4. In Figure 1, we show a schematic workflow of the entire process.

3 Results

We initiate the discussion of our results by showing that PageRank centralities capture age-related changes in Section 3.1. We leverage this finding to develop a framework for brain-age prediction in Section 3.2. Next, we present a comparison across different centrality measures in Section 3.3. Finally, we close out this section with

a comparison with other (non-network-based) approaches from literatures in Section $3.4\,$

3.1 Aging-related changes to the brain is reflected in network metrics of functional networks

In this result, we demonstrate that node centrality measures computed independently for each subject's functional MRI, capture information on changing functional activity caused by changes to underlying anatomical structures. Moreover, this behavior remains consistent across a cohort spanning decades of the human lifespan. As mentioned earlier, we use PageRank as the metric of choice due to the insights that may be gleaned by studying changes to stationary probability distributions of random walks on functional brain networks.

Once the dataset is suitably preprocessed, we compute the PageR-ank centrality for each subject and task condition as described in Section 2.3. We visualize the dataset in Figure 2. The colors of each data point indicate the age of the corresponding subject. In each task condition, the data points are arranged according to their brain age. The visually smooth transition across age suggests that the data-points may form clusters and lie on low-dimensional manifolds

Next, we compute the k-NN graph on the dataset with each node corresponding to a subject. We compute the Graph Laplacian (L=D-A) for this graph and its Fiedler Vector. We partition this dataset graph into two clusters using the Fiedler Vector (i.e., the eigen vector corresponding to the smallest non-zero eigenvalue of L). The results are visualized in Figure 3. We see that the Fiedler Vector of the dataset graph can be used to partition subjects into two clusters, that can roughly be characterized as "young" and "old". Across the three task conditions, the ages for the two clusters were 42.05 ± 14.13 and 67.25 ± 13.78 respectively.

To determine the optimal number clusters, we computed cluster evaluation metrics for k-means with $k=\{1,\ldots,40\}$. In Figure 4, we can see that for the three task conditions, the optimal value of $k\approx 20$ for Silhouette Value. This was in close agreement with Gap Statistics and the Davies-Bouldin Index. Larger values of k(>20) did not improve the downstream prediction accuracy, however smaller values of k(<18) increased error in age prediction. Thus, we fix k=20. In the next result, we use these age-specific clusters to predict the brain age of subjects.

3.2 Population-level Network Analysis Leads to Accurate Age Prediction

Method	MAE
Linear Regression	14.73 ± 11.76
Support Vector Regression	15.66 ± 10.92
(with Gaussian Kernel)	

Table 1: Baseline Mean Absolute Errors. This table summarizes the Mean Absolute Error (MAE) by baseline methods across three tasks (Rest, Sensorimotor, and Movie) in the CAM-CAN dataset.

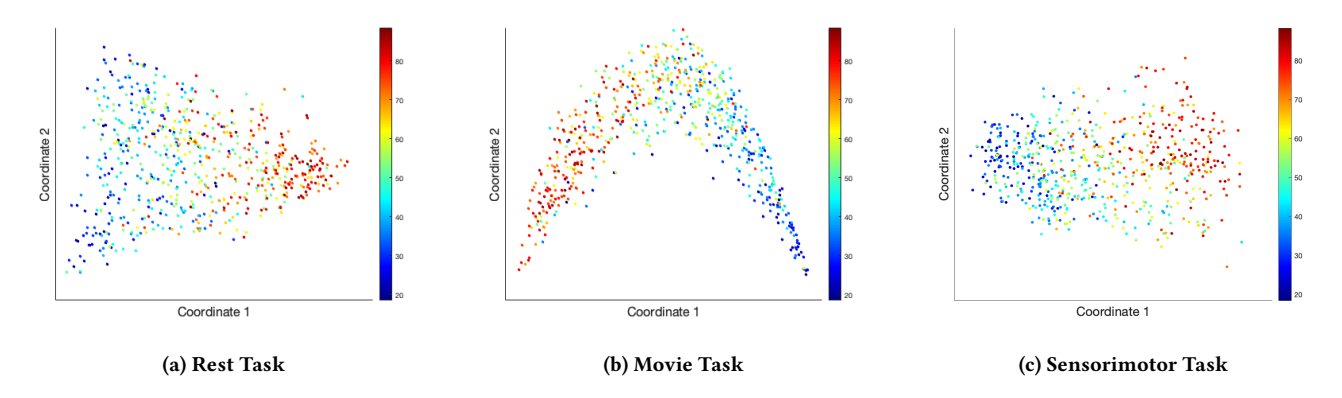


Figure 2: Pagerank centralities encode age-related features. In this figure, we demonstrate the heterogeneity in PageRank vectors corresponding to subjects ages 18 through 88 across three task conditions – rest, movie viewing, and sensorimotor activity. The colors of each data-point indicate the age of the corresponding subject. The graphs show that changes due to age are indeed reflected in PageRank vectors. For visualization, we reduce each data-point to two dimensions using Diffusion Maps. Similar trends can be visualized with other non-linear dimensionality reduction techniques such as t-SNE and UMAP (see Supplementary Material).

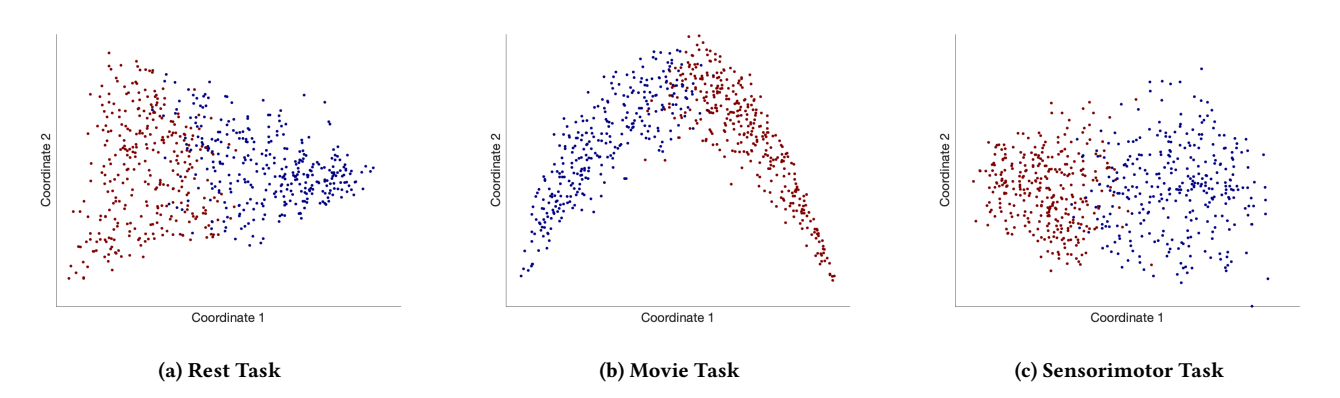


Figure 3: Pagerank centralities encode age-related features – contd. In this figure, we find clusters in the dataset using the Fiedler Vector. The cluster boundary we see in this figure is in line with the trend in ages seen in Figure 2. Moreover, the clusters can be found in low-dimensional manifolds. For the purposes of visualization, we reduce each data-point to two dimensions using Diffusion Maps. Similar trends can be visualized with other non-linear dimensionality reduction techniques such as t-SNE and UMAP.

In this result, we further bolster our hypothesis that brain network centrality measures encode age-specific information. To do so, we use the previously computed PageRank centrality vectors for all subjects to predict the age of each subject. As a baseline for the predictions obtained from our approach, we report Mean Absolute Errors (MAE) across three tasks for Linear Regression and Support Vector Regression in Table 1

Using the PageRank centralities computed from each functional image, we perform spectral clustering as described in Section 2.4. We set k=20, guided by the cluster evaluation metrics discussed in the previous results (Section 3.1). We order the medians of each cluster according to age and compute the ordering provided by the pseudotime procedure discussed in Section 2.4. We note that we are only using the age-labels of these cluster centers and not those of other subjects. We repeat this procedure in a leave-one-out fashion.

In each iteration, we leave one subject out of the clustering and pseudotime ordering procedure. We project the test subject onto the edges connecting the closest cluster center and select the edge with the higher projection (i.e., the more similar edge). We use the edge as a linear interpolation between the ages of the nodes (cluster centers) on either side. The average prediction error across all tasks was 4.08 ± 0.31 years, which is significantly better than the baseline. We visualize the actual age (red) and predicted age (blue) for each task in Figure 5. We also show the MAE for different age cohorts in Table 2. In both cases, we see a deviation in expected output for the oldest cohort (78-88) – in Figure 5, we see that the predictions in this age range is consistently lower than the chronological age, and in Table 2, we see a corresponding increase in MAE. We believe this could be due to an acceleration in age-related changes that is specific to individuals. Further study is required to ascertain

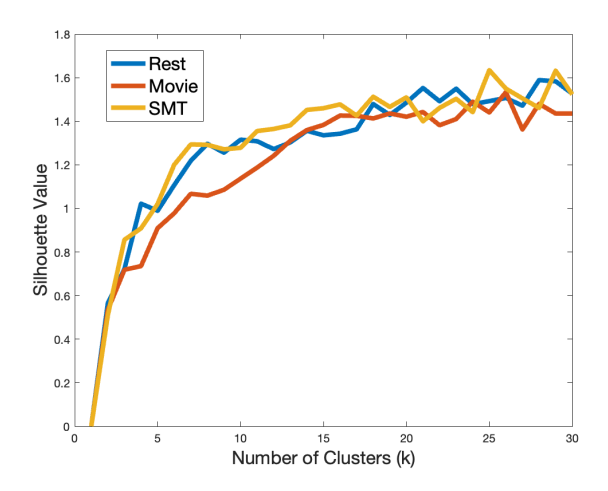


Figure 4: Cluster Evaluation Metric for different number of clusters. In this plot, we show the values for Silhouette Values for different values of k. This suggests that the optimal number of clusters is approximately 20. Similar plots were observed with Gap Statistic and Davies-Bouldin Index

the reason for this deviation. Finally, we report that there is no significant change in MAE for male v/s female and handedness.

Age Range	MAE
18-27	4.29
28-37	3.39
38-47	3.32
48-57	3.29
58-67	3.28
68-77	4.64
78-88	7.08

Table 2: Mean Absolute Errors across age. This table summarizes the Mean Absolute Error (MAE) for different age cohorts. Our results are largely stable from 18-77. However, the increase in error for ages 78-88 may be attributed to significant age-related functional changes.

3.3 Comparison of different Node Centrality Metrics

In this result, we compare the performance in age prediction using different network centrality measures. In addition to PageRank, we compare with a) degree centrality, b) eigenvector centrality, and c) betweenness centrality for each task. As before, we perform our analysis in a leave-one-out fashion. We compute the different centrality measures for each subject and each task. We then perform spectral clustering and predict trajectories (orderings) using the different centrality measures. To demonstrate the stability of the entire approach, we repeat the trajectory analysis 10^3 times.

The results are summarized in Figure 6. For each task, we see that the error obtained by PageRank is significantly lesser than

those obtained by degree, eigenvector, and betweenness centrality. The MAE in the four cases are 4.08 ± 0.31 , 7.73 ± 0.29 , 8.91 ± 0.33 , and 11.17 ± 0.38 . We explain the difference in results as follows: degree centrality is a local measure, and so is not informed by the overall network topology. Eigenvector centrality does not account for degrees of neighbors and does not incorporate a damping factor/follow probability. This seems to make it a weaker representation of predicting age. Finally, betweenness centrality measures the number of times a node appears in the shortest path between all pairs of nodes, and this does not seem to change significantly with age.

3.4 Comparison with Other Approaches

In this final set of results, we compare our results with other competing approaches available from literature. Table 3 lists the different methods, the age-range of the dataset on which the results were reported, and the Mean Absolute Error (MAE) in predicting brain age. On whole life-span datasets, the results obtained from our method (\approx 4 years) is clearly an advancement over other approaches.

We note that results demonstrated on datasets restricted to young individuals perform slightly better, particularly the method due to Li et al. [13]. However, when normalized across the age-range, our method gives 5.7%, whereas the method due to Li et al. yields 15.4% error. This result strongly suggests that network abstractions of functional neuroimages are powerful models to characterize aging-related changes in the brain.

4 Related Literature

Graph properties of functional and structural images of the brain have long been a topic of research [24][25][30]. While structural images have been used significantly to predict brain ages (ex: [18, 32]), we focus on methodologies that use functional images to understand age-dependent changes.

Zuo et al. [34] used rs-fMRI data to demonstrate a correlation between the voxel-level activity of the brain and age Using different centrality measures. Vergun et al. [29] explored the effectiveness of machine learning methods in age prediction. They applied SVMs to distinguish individuals by age (84% accuracy) and SVRs to predict chronological age using functional connectivity MRI data. Their results showed that an SVM classifier discriminated between young and old subjects with 84% accuracy. Monti et al. [15] proposed an approach that combines PCA to identify consistent functional connectivity networks across subjects with linear regression models to estimate brain age. They called this approach "Modular Hierarchical Analysis" (MHA). Using the CamCAN dataset, their approach predicted brain age with MAE of \approx 12 years. Similarly, Zhai et al. [31] used PCA to identify components related to age, and then they used these components as predictors in various regression models to estimate brain age. Smyser et al. [23] used SVMs to classify terms from preterm infants with 84% accuracy.

Deep learning methods have also shown promise in predicting brain age. Li et al. [13] developed a CNN model to learn features from whole-brain functional connectivity measures in subjects aged 8 to 22. Chang et al. [3] analyzed rsfMRI data from 176 healthy adults aged 18 to 78. Using Lasso error, they identify 39 key functional connections predictive of age. Deviations in the Default Mode Network

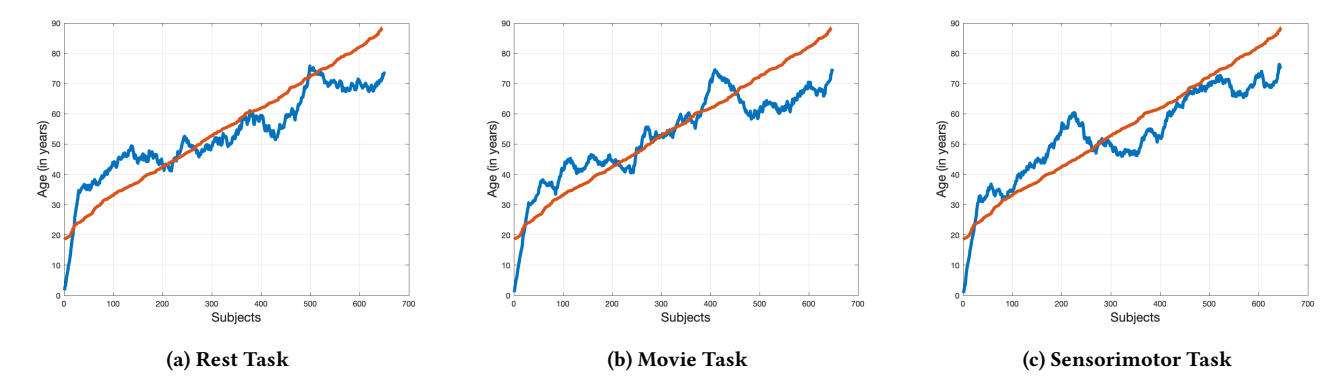


Figure 5: $Prediction\ of\ Brain\ Age\ In\ this\ figure,$ we show results for predicting brain age using the pseudotime-ordering method. Briefly, we cluster subjects into k clusters using spectral clustering, order the cluster centers according to age, and project each data point onto an edge between consecutive data-points. We use the projections to create an ordering of subjects and compare them with the actual ages.

Method	Age-Range	MAE
Ordinary Least Squares [31]	life-span	14.2
Modular Hierarchical Analysis (MHA) [15]	life-span	≈ 12
Support Vector Regression [31]	life-span	11.4
Lasso Regression [31]	life-span	9.2
This paper	life-span	4.08
Partial Least Squares[19]	young	4.7
Ordinary Least Squares[14]	young	4.27
CNN [13]	young	2.15

Table 3: Summary of results pertaining to errors in age prediction. This table summarizes the Mean Absolute Error (MAE) obtained by different methods. We separate the results according to age-range of participants. The lower MAE for young adults can be explained by the fact that the age range is typically around 15 years, whereas the age-range for lifespan is about 70 years.

(DMN) were linked to abnormal aging patterns, suggesting that functional connectivity within the DMN may serve as a biomarker for early detection of atypical brain aging, even before cognitive decline becomes apparent. While they report an MAE of 2.48 years in age prediction, it was achieved only after removing 68 subjects deemed as "outliers". On the whole, their reported MAE was 12.32 years.

Baghernezhad and Daliri [1] investigated age-related changes in human brain functional connectivity using graph theory and machine learning techniques on rsfMRI data. Their research revealed that aging is associated with alterations in network centrality measures. Using a decision-tree classifier, they were able to classify each subject into 8 to 15 years, 25 to 35 years, and 45 to 75 years with an accuracy of 82.2%. Hardy et al. [8] utilized magnetoencephalography (MEG) to study spontaneous oscillations and functional coupling in resting-state brain networks across the adult lifespan. Their findings underscored the potential of MEG in capturing age-related changes in brain function, offering a complementary perspective to fMRI-based analyses. Farahani et al. [6] reviewed the application of graph theory to study network alterations associated with aging, summarizing different methodological advancements and insights gained from this approach. Taimouri and Ravindra [26] showed that a small subset of edges in the functional connectome remain

stable across healthy aging. Kumari and Sundarrajan [11] review methods that use structural images.

These studies collectively highlight the growing interest and advancements in leveraging network centrality measures, graph theoretical frameworks, machine learning, and deep learning techniques to understand and predict the effects of aging on brain connectivity. Such efforts are instrumental in uncovering biomarkers for typical and atypical brain aging, contributing to our understanding of neural and cognitive health across the lifespan.

5 Conclusion and Discussion

In this paper, we demonstrate a new method to predict brain age using graph centrality properties of functional networks. Our approach yielded an MAE of 4.08 ± 0.31 years, which is significantly better than other methods operating on datasets across the human lifespan (Table 3). Our results are comparable to those reported on datasets with narrower age ranges (i.e., on adolescents and young adults). Furthermore, our method does not rely on knowledge of specific functional networks or their roles in aging. Instead, we prescribe an entirely data-driven approach that uses network properties to represent each functional image, and then use this framework to find an ordering of subjects. We show that this ordering is consistent with the ages of the population.

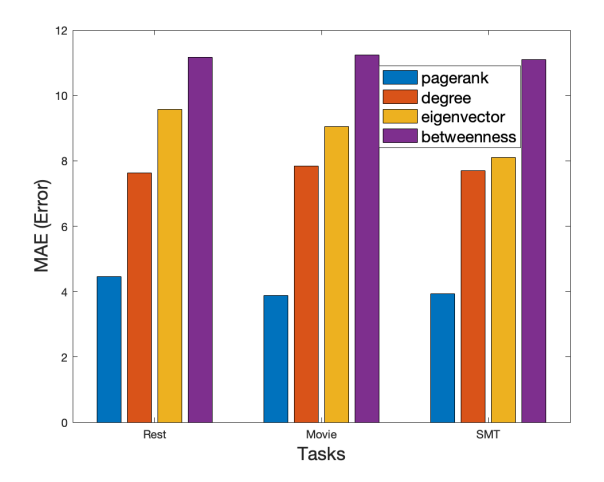


Figure 6: Age Prediction for different centrality measures. This bar-plot shows the mean absolute error for three tasks (rest, movie-viewing, and sensorimotor) and four centrality measures (PageRank, degree, eigenvector, and betweenness). For each task, PageRank is the best centrality measure. Errorbars for each plot were > 0.4, and so were omitted.

Although our current analysis focuses exclusively on healthy aging, future work will evaluate whether the network centrality changes observed here are preserved or altered in neurodegenerative diseases such as Alzheimer's and Parkinson's. Longitudinal datasets containing both healthy controls and patients would allow us to disentangle changes associated with normal aging from those arising due to pathology, and to determine whether deviations from the healthy trajectory could serve as early biomarkers of disease.

Multimodal integration presents another promising extension. By combining structural and functional images, we could create a unified representation of brain networks, potentially capturing complementary information and improving prediction accuracy. This multimodal approach could provide richer inputs that enhance our ability to characterize both healthy and pathological brain aging.

In addition, applying our model to new datasets will require careful harmonization across imaging protocols. Differences in scanner hardware, acquisition parameters (e.g., TR, spatial resolution, number of volumes), or experimental conditions (e.g., rest vs. task) can introduce systematic biases that degrade performance. However, batch-effect correction methods such as ComBat, functional connectivity normalization, or site/scanner harmonization strategies can mitigate these effects. For datasets with substantially different paradigms, fine-tuning the model on a small labeled subset may be necessary. In principle, new data can be integrated by recomputing centrality measures and projecting them into the existing pseudotime space, provided that preprocessing and normalization steps are consistent with the original training.

References

 Sepideh Baghernezhad and Mohammad Reza Daliri. 2024. Age-related changes in human brain functional connectivity using graph theory and machine learning

- techniques in resting-state fMRI data. GeroScience (2024), 1-18.
- [2] Suvarna Saumya Chandrashekhar, Mashrin Srivastava, B Jaganathan, and Pankaj Shukla. 2022. PageRank Algorithm using Eigenvector Centrality–New Approach. arXiv preprint arXiv:2201.05469 (2022).
- [3] Jose Ramon Chang, Zai-Fu Yao, Shulan Hsieh, and Torbjörn EM Nordling. 2024. Age Prediction Using Resting-State Functional MRI. Neuroinformatics 22, 2 (2024), 119–134.
- [4] R Cameron Craddock, G Andrew James, Paul E Holtzheimer III, Xiaoping P Hu, and Helen S Mayberg. 2012. A whole brain fMRI atlas generated via spatially constrained spectral clustering. *Human brain mapping* 33, 8 (2012), 1914–1928.
- [5] Jessica S Damoiseaux. 2017. Effects of aging on functional and structural brain connectivity. Neuroimage 160 (2017), 32–40.
- [6] Farzad V Farahani, Waldemar Karwowski, and Nichole R Lighthall. 2019. Application of graph theory for identifying connectivity patterns in human brain networks: a systematic review. frontiers in Neuroscience 13 (2019), 585.
- [7] Kathleen A Garrison, Dustin Scheinost, Emily S Finn, Xilin Shen, and R Todd Constable. 2015. The (in) stability of functional brain network measures across thresholds. *Neuroimage* 118 (2015), 651–661.
- [8] Samuel Hardy, Gill Roberts, Matthew Ventresca, and Benjamin T Dunkley. 2024. Predicting brain age across the adult lifespan with spontaneous oscillations and functional coupling in resting brain networks captured with magnetoencephalography. *Imaging Neuroscience* (2024).
- [9] Zhicheng Ji and Hongkai Ji. 2016. TSCAN: Pseudo-time reconstruction and evaluation in single-cell RNA-seq analysis. *Nucleic acids research* 44, 13 (2016), e117–e117.
- [10] Tania S Kong, Caterina Gratton, Kathy A Low, Chin Hong Tan, Antonio M Chiarelli, Mark A Fletcher, Benjamin Zimmerman, Edward L Maclin, Bradley P Sutton, Gabriele Gratton, et al. 2020. Age-related differences in functional brain network segregation are consistent with a cascade of cerebrovascular, structural, and cognitive effects. Network Neuroscience 4, 1 (2020), 89–114.
- [11] LK Soumya Kumari and R Sundarrajan. 2024. A review on brain age prediction models. Brain Research 1823 (2024), 148668.
- [12] Anvar Kurmukov, Ayagoz Mussabaeva, Yulia Denisova, Daniel Moyer, Neda Jahanshad, Paul M Thompson, and Boris A Gutman. 2020. Optimizing connectivity-driven brain parcellation using ensemble clustering. *Brain Connectivity* 10, 4 (2020). 183–194.
- [13] Hongming Li, Theodore D Satterthwaite, and Yong Fan. 2018. Brain age prediction based on resting-state functional connectivity patterns using convolutional neural networks. In 2018 ieee 15th international symposium on biomedical imaging (isbi 2018). IEEE, 101–104.
- [14] Martina J Lund, Dag Alnæs, Ann-Marie G de Lange, Ole A Andreassen, Lars T Westlye, and Tobias Kaufmann. 2022. Brain age prediction using fMRI network coupling in youths and associations with psychiatric symptoms. NeuroImage: Clinical 33 (2022). 102921.
- [15] Ricardo Pio Monti, Alex Gibberd, Sandipan Roy, Matthew Nunes, Romy Lorenz, Robert Leech, Takeshi Ogawa, Motoaki Kawanabe, and Aapo Hyvärinen. 2020. Interpretable brain age prediction using linear latent variable models of functional connectivity. Plos one 15, 6 (2020), e0232296.
- [16] Mark Newman. 2018. Networks. Oxford university press.
- [17] Lawrence Page. 1999. The PageRank citation ranking: Bringing order to the web. Technical Report. Technical Report.
- [18] Oscar Pina, Irene Cumplido-Mayoral, Raffaele Cacciaglia, José María González-de Echávarri, Juan Domingo Gispert, and Verónica Vilaplana. 2022. Structural networks for brain age prediction. In International Conference on Medical Imaging with Deep Learning. PMLR, 944–960.
- [19] Jian Qin, Shan-Guang Chen, Dewen Hu, Ling-Li Zeng, Yi-Ming Fan, Xiao-Ping Chen, and Hui Shen. 2015. Predicting individual brain maturity using dynamic functional connectivity. Frontiers in human neuroscience 9 (2015), 418.
- [20] Vikram Ravindra, Huda Nassar, David F Gleich, and Ananth Grama. 2019. Rigid graph alignment. In International conference on complex networks and their applications. Springer, 621-632.
- [21] Vikram Ravindra, Huda Nassar, David F Gleich, and Ananth Grama. 2022. Aligning spatially constrained graphs. IEEE Transactions on Knowledge and Data Engineering 35, 8 (2022), 7712–7723.
- [22] Meredith A Shafto, Lorraine K Tyler, Marie Dixon, Jason R Taylor, James B Rowe, Rhodri Cusack, Andrew J Calder, William D Marslen-Wilson, John Duncan, Tim Dalgleish, et al. 2014. The Cambridge Centre for Ageing and Neuroscience (Cam-CAN) study protocol: a cross-sectional, lifespan, multidisciplinary examination of healthy cognitive ageing. BMC neurology 14 (2014), 1–25.
- [23] Christopher D Smyser, Nico UF Dosenbach, Tara A Smyser, Abraham Z Snyder, Cynthia E Rogers, Terrie E Inder, Bradley L Schlaggar, and Jeffrey J Neil. 2016. Prediction of brain maturity in infants using machine-learning algorithms. NeuroImage 136 (2016), 1–9.
- [24] Olaf Sporns. 2003. Graph theory methods for the analysis of neural connectivity patterns. Neuroscience databases: A practical guide (2003), 171–185.
- [25] Olaf Sporns. 2018. Graph theory methods: applications in brain networks. Dialogues in clinical neuroscience 20, 2 (2018), 111–121.

- [26] Monireh Taimouri and Vikram Ravindra. 2025. Characterizing changes to individual-specific brain signature with age. Frontiers in Aging Neuroscience 17 (2025), 1493855.
- [27] Jason R Taylor, Nitin Williams, Rhodri Cusack, Tibor Auer, Meredith A Shafto, Marie Dixon, Lorraine K Tyler, Richard N Henson, et al. 2017. The Cambridge Centre for Ageing and Neuroscience (Cam-CAN) data repository: Structural and functional MRI, MEG, and cognitive data from a cross-sectional adult lifespan sample. neuroimage 144 (2017), 262–269.
- [28] Cole Trapnell, Davide Cacchiarelli, Jonna Grimsby, Prapti Pokharel, Shuqiang Li, Michael Morse, Niall J Lennon, Kenneth J Livak, Tarjei S Mikkelsen, and John L Rinn. 2014. The dynamics and regulators of cell fate decisions are revealed by pseudotemporal ordering of single cells. *Nature biotechnology* 32, 4 (2014), 381–386.
- [29] Svyatoslav Vergun, Alok S Deshpande, Timothy B Meier, Jie Song, Dana L Tudorascu, Veena A Nair, Vikas Singh, Bharat B Biswal, M Elizabeth Meyerand, Rasmus M Birn, et al. 2013. Characterizing functional connectivity differences in aging adults using machine learning on resting state fMRI data. Frontiers in

- $computational\ neuroscience\ 7\ (2013),\ 38.$
- [30] Xin Wu and Yufang Zhao. 2021. Degree Centrality of a Brain Network Is Altered by Stereotype Threat: Evidences From a Resting-State Functional Magnetic Resonance Imaging Study. Frontiers in Psychology 12 (2021), 705363.
- [31] Jian Zhai and Ke Li. 2019. Predicting brain age based on spatial and temporal features of human brain functional networks. Frontiers in human neuroscience 13 (2019), 62.
- [32] Hui Zhang, Peng Cao, Henry KF Mak, and Edward S Hui. 2024. The structural-functional-connectivity coupling of the aging brain. GeroScience (2024), 1–13.
- [33] Tengda Zhao, Miao Cao, Haijing Niu, Xi-Nian Zuo, Alan Evans, Yong He, Qi Dong, and Ni Shu. 2015. Age-related changes in the topological organization of the white matter structural connectome across the human lifespan. *Human brain mapping* 36, 10 (2015), 3777–3792.
- [34] Xi-Nian Zuo, Ross Ehmke, Maarten Mennes, Davide Imperati, F Xavier Castellanos, Olaf Sporns, and Michael P Milham. 2012. Network centrality in the human functional connectome. *Cerebral cortex* 22, 8 (2012), 1862–1875.